Electronic supplementary materials

For https://doi.org/10.1631/jzus.A2500019

Fast prediction of vibration source intensity induced by metro trains moving on regular and floating slab tracks

Lihui XU[1]✉, Meng GAO[1], Xinyu TAN[2], Chao ZOU[3], Meng MA[4]

[1]*College of Civil Engineering and Architecture, Shandong University of Science and Technology, Qingdao 266590, China*
[2]*National Engineering Research Center for Digital Construction and Evaluation Technology of Urban Rail Transit, China Railway Design Corporation, Tianjin 300308, China*
[3]*School of Civil and Transportation Engineering, Guangdong University of Technology, Guangzhou 510006, China*
[4]*Key Laboratory of Urban Underground Engineering of Ministry of Education, Beijing Jiaotong University, Beijing 100044, China*

✉Corresponding author: Lihui XU, Xlh@sdust.edu.cn

Section S1 Analytical prediction model for vibration source intensity

S1.1 Model overview

Fig. S1 presents an overview of the train-track-tunnel-soil system, featuring both regular and floating slab tracks. In the calculations, the whole system is divided into two subsystems, incorporating the train-track subsystem and the track-tunnel-soil subsystem. The coupling of the above subsystems is accomplished by the transmission of supporting forces, which refer to the forces transmitted through fasteners from the rails to either the roadbed slab or the floating slab.

The train-track subsystem is analytically modeled by Ma (2015) using the periodic structure theory and supplies the supporting forces of fasteners. In this part, a single vehicle is treated as the rigid body, possessing 10 degrees of freedom, which include the vertical movements of the train body, two bogies, and four wheelsets, along with the rotations of the train body and two bogies. The rails and floating slabs are represented using the Euler beam model. The fasteners are modeled by spring-damper elements, and isolators of the floating slabs and track substructures are represented by continuous springs. The detailed derivations are referred to in the literature (Ma, 2015).

In the track-tunnel-soil subsystem with the regular slab track, the supporting forces are discretely distributed upon the track slab with the spacing of L=0.6 m, corresponding to the spacing of fasteners or sleepers. Ma (2015) demonstrated that the forces of fasteners adhere to a periodicity relationship, resulting in the periodic nature of the subsystem. Although the floating slab is constructed in a discontinuous manner, the presence of shear hinges between adjacent slabs allows it to be treated as a continuous slab, as illustrated in Fig. S1. Therefore, a similar periodicity exists. In both cases, the tunnel-soil system is modeled by the periodic PiP model. Both the roadbed slab and the floating slab are modeled as Euler beams. The interactions between the components are facilitated by continuous springs. Rails are excluded in this subsystem.

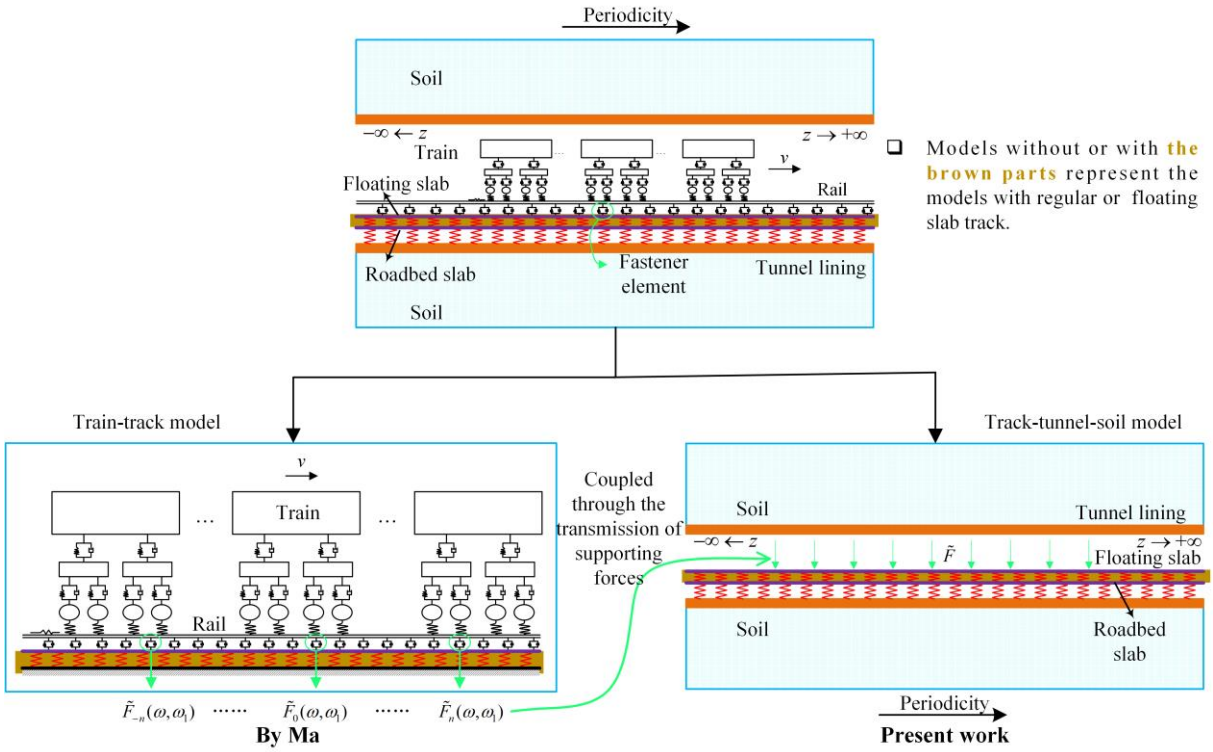

Fig. S1 Overview of the train-track-tunnel-soil system with regular or floating slab track.

S1.2 Periodic PiP model

Fig. S2 gives the schematic diagram of the periodic PiP model. The tunnel lining is represented as an infinitely long Flügge circular shell (r=R) (Flügge, 1973), while the surrounding soil is modeled as continuum media in a full space with a hollow ($r_s \in [R, \infty)$). It is assumed that the presence of a free surface on the ground has no impact on the responses of the tunnel, which was first adopted by M.F.M. Hussein et al. (2014) to predict the ground surface response and good results were obtained. The forces from the roadbed slab beam are conveyed to the tunnel invert through the springs. The PiP model by Forrest and Hunt (2006) is expanded into a periodic PiP model, considering the periodicity of the supporting forces.

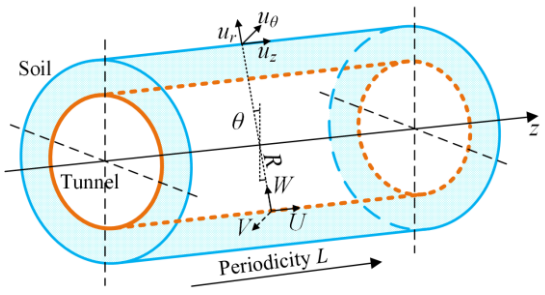

Fig. S2 Schematic diagram of the periodic PiP model.

Considering a moving periodic load with a periodicity length of L in the z direction, a frequency of ω_l, and a speed of v, the responses $\Theta(z,t)$ of two adjacent points in the structure, with a spacing of L, adhere to the following relationship,

$$\Theta(z+L,t+L/v) = \mathrm{e}^{\mathrm{i}\omega_l L/v}\Theta(z,t) \tag{S1}$$

By performing a Fourier transform regarding time t in Eq. (S1), the responses in the frequency domain can be represented as a summation of the generalized modal functions,

$$\tilde{\Theta}\left(z,\omega,\omega_1\right)=\sum_{n=-\infty}^{n=+\infty}\tilde{\Theta}_n\left(\omega\right)\Phi_n\left(z,\omega_1,\omega\right) \tag{S2}$$

where $\Phi_n\left(z,\omega_1,\omega\right)=\mathrm{e}^{\mathrm{i}\lambda_n z}$ is the generalized modal function, $\lambda_n=\dfrac{2\pi n}{L}+\dfrac{\omega_1-\omega}{v}$. $\tilde{\Theta}_n\left(\omega\right)$ represents the modal coefficients. ω denotes the response frequency. The symbol ~ represents the quantity in the frequency domain.

There are three equilibrium equations regarding the longitudinal z, circumferential θ, and radial r directions in the Flügge shell. By performing a Fourier transform regarding time t, a modal decomposition regarding coordinate z, and a trigonometric decomposition regarding coordinate θ, the relationship between displacements and tractions in the frequency-wavenumber domain can be derived,

$$\boldsymbol{A}_{\mathrm{E}}\tilde{\boldsymbol{U}}_{nm}=\frac{Eh}{-R\left(1-\nu^2\right)}\boldsymbol{A}\begin{Bmatrix}\tilde{U}_{nm}\\ \tilde{V}_{nm}\\ \tilde{W}_{nm}\end{Bmatrix}=\begin{Bmatrix}\tilde{Q}_{znm}\\ \tilde{Q}_{\theta nm}\\ \tilde{Q}_{rnm}\end{Bmatrix}=\tilde{\boldsymbol{Q}}_{nm} \tag{S3}$$

where $\tilde{\boldsymbol{U}}_{nm}$ and $\tilde{\boldsymbol{Q}}_{nm}$ are the tunnel displacement and tractions vector. The subscripts n and m represent the modal order and trigonometric series order. E, h, and ν are the elastic modulus, lining thickness, and Poisson's ratio, respectively. $\boldsymbol{A}_{\mathrm{E}}=\dfrac{Eh}{-R\left(1-\nu^2\right)}\boldsymbol{A}$ is a 3×3 coefficient matrix. The elements of matrix $\boldsymbol{A}$ are referred to in literature (Forrest and Hunt, 2006), where the wavenumber ξ in the original expressions should be replaced by λ_n for a periodicity sense.

In the elastodynamic equations of the soil medium, a decomposition using potential functions is conducted to derive the uncoupled equations. Subsequently, by applying the Fourier transform, modal decomposition, and trigonometric decomposition, the general solutions of soil displacements and stresses in the cylindrical coordinate can be formulated in the frequency-wavenumber domain (Xu and Ma, 2023). It should be noted that only outgoing cylindrical waves exist in the full space of soil. The displacements $\tilde{\boldsymbol{u}}_{nm}$ and stresses $\tilde{\boldsymbol{t}}_{nm}$ at the interface $r=R$ have the following forms,

$$\tilde{\boldsymbol{u}}_{nm}=\begin{Bmatrix}\tilde{u}_{znm}\\ \tilde{u}_{\theta nm}\\ -\tilde{u}_{rnm}\end{Bmatrix}=\begin{bmatrix}\chi_{\mathrm{o}31} & \chi_{\mathrm{o}32} & \chi_{\mathrm{o}33}\\ \chi_{\mathrm{o}21} & \chi_{\mathrm{o}22} & \chi_{\mathrm{o}23}\\ -\chi_{\mathrm{o}11} & -\chi_{\mathrm{o}12} & -\chi_{\mathrm{o}13}\end{bmatrix}_{r=R}\begin{Bmatrix}B_{\mathrm{o}1nm}\\ B_{\mathrm{o}2nm}\\ B_{\mathrm{o}3nm}\end{Bmatrix}=\boldsymbol{\chi}_{\mathrm{o}}(r=R)\boldsymbol{B}_{onm} \tag{S4}$$

$$\tilde{\boldsymbol{t}}_{nm}=\begin{Bmatrix}-\sigma_{rznm}\\ -\sigma_{r\theta nm}\\ \sigma_{rrnm}\end{Bmatrix}=\begin{bmatrix}-\eta_{\mathrm{o}31} & -\eta_{\mathrm{o}32} & -\eta_{\mathrm{o}33}\\ -\eta_{\mathrm{o}21} & -\eta_{\mathrm{o}22} & -\eta_{\mathrm{o}23}\\ \eta_{\mathrm{o}11} & \eta_{\mathrm{o}12} & \eta_{\mathrm{o}13}\end{bmatrix}_{r=R}\begin{Bmatrix}B_{\mathrm{o}1nm}\\ B_{\mathrm{o}2nm}\\ B_{\mathrm{o}3nm}\end{Bmatrix}=\boldsymbol{\eta}_{\mathrm{o}}(r=R)\boldsymbol{B}_{onm} \tag{S5}$$

where the expressions of χ_{oij} and η_{oij} (i,j=1,2,3) are referred to in literature (Xu and Ma, 2023) and listed in the following. The subscript o represents the outgoing wave. $\boldsymbol{B}_{\mathrm{o}}$ is the unknown coefficient vector. The negative sign in the expressions is to keep the displacement and stress directions of soil consistent with those of the shell.

The expressions of χ_{oij} (i,j=1,2,3) take the following forms,

$$\chi_{\mathrm{o}11}=k_{\mathrm{rp}}H_m^{(1)\prime}(k_{\mathrm{rp}}r)\,,\quad \chi_{\mathrm{o}12}=\frac{m}{r}H_m^{(1)}(k_{\mathrm{rs}}r)\,,\quad \chi_{\mathrm{o}13}=\mathrm{i}k_{\mathrm{rs}}\lambda_n H_m^{(1)\prime}(k_{\mathrm{rs}}r)$$

$$\chi_{\mathrm{o}21}=-\frac{m}{r}H_m^{(1)}(k_{\mathrm{rp}}r)\,,\quad \chi_{\mathrm{o}22}=-k_{\mathrm{rs}}H_m^{(1)\prime}(k_{\mathrm{rs}}r)\,,\quad \chi_{\mathrm{o}23}=-\mathrm{i}\lambda_n\frac{m}{r}H_m^{(1)}(k_{\mathrm{rs}}r)$$

$$\chi_{\mathrm{o}31}=\mathrm{i}\lambda_n H_m^{(1)}(k_{\mathrm{rp}}r)\,,\quad \chi_{\mathrm{o}32}=0\,,\quad \chi_{\mathrm{o}33}=k_{\mathrm{rs}}^2H_m^{(1)}(k_{\mathrm{rs}}r) \tag{S6}$$

The expressions of η_{oij} (i,j=1,2,3) take the following forms,

$$\eta_{\mathrm{o}11}=\mu\left[(2k_{\mathrm{p}}^2-k_{\mathrm{s}}^2)H_m^{(1)}(k_{\mathrm{rp}}r)+2k_{\mathrm{rp}}^2H_m^{(1)\prime\prime}(k_{\mathrm{rp}}r)\right]$$

$$\eta_{\mathrm{o}12}=\frac{2\mu m}{r^2}\left[k_{\mathrm{rs}}rH_m^{(1)\prime}(k_{\mathrm{rs}}r)-H_m^{(1)}(k_{\mathrm{rs}}r)\right]$$

$$\eta_{\mathrm{o}13}=2\mathrm{i}\mu\lambda_n k_{\mathrm{rs}}^2H_m^{(1)\prime\prime}(k_{\mathrm{rs}}r)$$

$$\eta_{\mathrm{o}21}=\frac{2\mu m}{r^2}\left[H_m^{(1)}(k_{\mathrm{rp}}r)-k_{\mathrm{rp}}rH_m^{(1)\prime}(k_{\mathrm{rp}}r)\right]$$

$$\eta_{\mathrm{o}22}=-\mu k_{\mathrm{rs}}^2\left[2H_m^{(1)\prime\prime}(k_{\mathrm{rs}}r)+H_m^{(1)}(k_{\mathrm{rs}}r)\right] \tag{S7}$$

$$\eta_{\mathrm{o}23}=\frac{2\mathrm{i}\mu\lambda_n m}{r^2}\left[H_m^{(1)}(k_{\mathrm{rs}}r)-k_{\mathrm{rs}}rH_m^{(1)\prime}(k_{\mathrm{rs}}r)\right]$$

$$\eta_{\mathrm{o}31}=2\mathrm{i}\mu\lambda_n k_{\mathrm{rp}}H_m^{(1)\prime}(k_{\mathrm{rp}}r)$$

$$\eta_{\mathrm{o}32}=\frac{\mathrm{i}\mu\lambda_n m}{r}H_m^{(1)}(k_{\mathrm{rs}}r)$$

$$\eta_{\mathrm{o}33}=\mu k_{\mathrm{rs}}(k_{\mathrm{rs}}^2-\lambda_n^2)H_m^{(1)\prime}(k_{\mathrm{rs}}r)$$

In these expressions, the subscripts p and s represent compressional and shear waves, respectively. The subscript r represents the radial direction. $k_{\mathrm{p,s}}=\omega/c_{\mathrm{p,s}}$ and $k_{\mathrm{rp,s}}=\pm\sqrt{\omega^2/c_{\mathrm{p,s}}^2-\lambda_n^2}$ are the wavenumbers, in which $c_{\mathrm{p,s}}$ is the compressional or shear wave velocity. μ is the Lamé constant. The function $H_m^{(1)}(\cdot)$ is the m-th order Hankel function of the first kind. The symbols $\bullet'$ and $\bullet''$ represent the first and second derivatives with respect to the whole argument ($k_{\mathrm{rp,s}}r$).

The tunnel shell and soil medium should satisfy the displacement compatibility and stress equilibrium conditions, yielding,

$$\tilde{\boldsymbol{U}}_{nm}=\tilde{\boldsymbol{u}}_{nm} \tag{S8}$$

$$\tilde{\boldsymbol{Q}}_{nm}+\tilde{\boldsymbol{t}}_{nm}=\begin{Bmatrix}\tilde{P}_{znm}\\ \tilde{P}_{\theta nm}\\ \tilde{P}_{rnm}\end{Bmatrix}=\tilde{\boldsymbol{P}}_{nm} \tag{S9}$$

where $\tilde{\boldsymbol{P}}_{nm}$ is the load vector.

Substituting Eqs (3)-(5) into Eqs (8) and (9), the tunnel displacement vector $\tilde{\boldsymbol{U}}_{nm}$ and soil known coefficient vector $\boldsymbol{B}_{onm}$ should satisfy the following equation,

$$\boldsymbol{K}_{nm}\tilde{\boldsymbol{U}}_{nm}^{B}=\begin{bmatrix}\boldsymbol{A}_{\mathrm{E}} & \boldsymbol{\eta}_{\mathrm{o}}(r=R)\\ \boldsymbol{I} & -\boldsymbol{\chi}_{\mathrm{o}}(r=R)\end{bmatrix}\begin{Bmatrix}\tilde{\boldsymbol{U}}_{nm}\\ \boldsymbol{B}_{onm}\end{Bmatrix}=\begin{Bmatrix}\tilde{\boldsymbol{P}}_{nm}\\ \boldsymbol{0}\end{Bmatrix}=\tilde{\boldsymbol{P}}_{nm}^{0} \tag{S10}$$

After solving Eq. (S10), the tunnel displacement $\tilde{\boldsymbol{U}}_{nm}$ can be obtained. The following formulation can be used to determine the soil displacement at a certain interface (r=a),

$$\tilde{\boldsymbol{u}}_{nm}=\boldsymbol{\chi}_{\mathrm{o}}(r=a)\boldsymbol{B}_{onm} \tag{S11}$$

According to the linear superposition principle, the tunnel displacement $\boldsymbol{U}$ in the time-space domain is expressed as,

$$\boldsymbol{U}=\begin{Bmatrix}U\\ V\\ W\end{Bmatrix}=\int_{-\infty}^{+\infty}\left\{\sum_{n=-\infty}^{n=\infty}\left(\sum_{m=0}^{m=+\infty}\tilde{\boldsymbol{U}}_{nm}\boldsymbol{S}_{m}\right)\boldsymbol{\Phi}_{n}\right\}\mathrm{e}^{\mathrm{i}\omega t}\mathrm{d}t \tag{S12}$$

where the matrix $\boldsymbol{S}_{m}=\mathrm{diag}(\cos m\theta,\sin m\theta,\cos m\theta)$ is diagonal.

So far, the PiP model has been developed into the periodic PiP model by utilizing the principles of periodicity theory.

S1.3 Analytical solution of regular slab

In this study, the regular track slab is simplified as the infinitely long Euler beam attached to the tunnel invert via the continuously distributed springs along the longitudinal direction in the periodic PiP model, as illustrated in Fig. S3. The slab beam is subjected to supporting forces from moving trains.

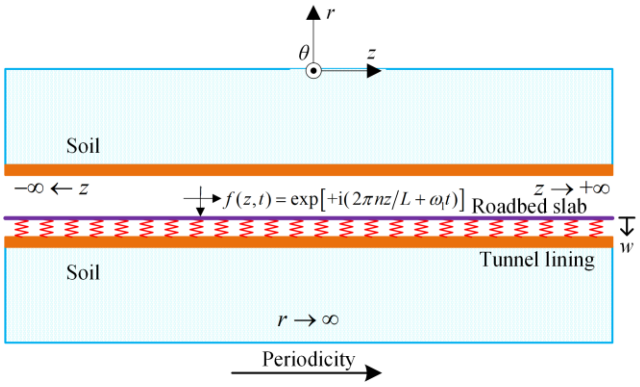

Fig. S3 Regular track slab attached to the tunnel invert in the periodic PiP model.

Assuming a periodic load $f(z,t)$ with a periodicity length L, a frequency ω_{l}, and a wavenumber n moving on the slab beam at a speed of v, the motion equation of the beam is,

$$m\frac{\partial^{2}w}{\partial t^{2}}+EI\frac{\partial^{4}w}{\partial z^{4}}+\left(w+W^{\dagger}\right)k_{\mathrm{eff}}=f(z,t) \tag{S13}$$

where w is the displacement of the roadbed slab beam. m is the mass per unit length. EI is the bending stiffness. $W^{\dagger}$ is the radial displacement at the tunnel invert (r=R, θ=π). k_{eff} represents the

effective stiffness of the equivalent spring that simulates the contacts between the roadbed and the tunnel invert.

By applying a Fourier transform regarding *t* and a modal decomposition regarding *z*, the solution is derived as,

$$\tilde{w}_n = \alpha \tilde{W}_n^{\dagger} + \tilde{\Delta}_n \tag{S14}$$

$$\alpha = \frac{-k_{\text{eff}}}{EI\lambda_n^4 - m\omega^2 + k_{\text{eff}}}, \tilde{\Delta}_n = \frac{\tilde{f}_n}{EI\lambda_n^4 - m\omega^2 + k_{\text{eff}}} \tag{S15}$$

where $\tilde{f}_n$ denotes the load in the frequency-wavenumber domain. The expression for a moving periodic load can be found in reference (Xu and Ma, 2023). The expression for a moving train load will be provided later.

The radial forces acting on the tunnel invert transmitted by the spring have the following form,

$$\tilde{P}_{rn} = -k_{\text{eff}}(\tilde{w}_n + \tilde{W}_n^{\dagger})\frac{(\theta - \pi)}{R} = -k_{\text{eff}}\left\{(1+\alpha)\tilde{W}_n^{\dagger} + \tilde{\Delta}_n\right\}\frac{(\theta - \pi)}{R} \tag{S16}$$

The terms $\tilde{W}_n^{\dagger}$ and $\delta(\theta - \pi)$ are expressed as,

$$\tilde{W}_n^{\dagger} = \sum_{m=0}^{m=+\infty} \tilde{W}_{nm}\cos m\theta\Big|_{\theta=\pi} = \left\{\boldsymbol{C}_0\ \boldsymbol{C}_1\ \cdots\ \boldsymbol{C}_M\right\}\begin{Bmatrix}\tilde{\boldsymbol{U}}_{n1}^B\\ \tilde{\boldsymbol{U}}_{n2}^B\\ \vdots\\ \tilde{\boldsymbol{U}}_{nM}^B\end{Bmatrix} = \boldsymbol{C}\tilde{\boldsymbol{U}}_n^B \tag{S17}$$

$$\delta(\theta - \pi) = \sum_{m=0}^{+\infty}\frac{\varepsilon_m}{2\pi}(-1)^m\cos m\theta \tag{S18}$$

where $\boldsymbol{C}_m = \{0\quad 0\quad \cos m\pi\quad 0\quad 0\quad 0\}$. Vector $\boldsymbol{C}$ has the dimensions of $1\times 6(M+1)$ and Vector $\tilde{\boldsymbol{U}}_n^B$ has the dimensions of $6(M+1)\times 1$. $\varepsilon_m = 1$ when m=0, and $\varepsilon_m = 2$ when m>0.

Substituting Eqs (17) and (18) into (16), the following expression is obtained,

$$\tilde{P}_{rn} = -k_{\text{eff}}\left\{(1+\alpha)\sum_{m=0}^{m=+\infty}\tilde{W}_{nm}\cos m\theta\Big|_{\theta=\pi} + \tilde{\Delta}_n\right\}\sum_{m=0}^{+\infty}\frac{\varepsilon_m}{2\pi R}(-1)^m\cos m\theta \tag{S19}$$

Accordingly, the load vector $\tilde{\boldsymbol{P}}_{nm}^0$ in Eq. (S10) can be formulated as,

$$\tilde{\boldsymbol{P}}_{nm}^0 = \tilde{P}_{rnm}\boldsymbol{E} = -k_{\text{eff}}(1+\alpha)\boldsymbol{V}_m\boldsymbol{C}\tilde{\boldsymbol{U}}_n^B - k_{\text{eff}}\tilde{\Delta}_n\boldsymbol{V}_m \tag{S20}$$

where $\boldsymbol{E}=\{0\ 0\ 1\ 0\ 0\ 0\}^{\mathrm{T}}$, $\boldsymbol{V}_m = \left\{0\quad 0\quad \frac{\varepsilon_m}{2\pi R}(-1)^m\quad 0\quad 0\quad 0\right\}^{\mathrm{T}}$.

Substituting Eq. (S20) into Eq. (S10) produces equilibrium equations for each *m*,

$$\boldsymbol{K}_{nm}\tilde{\boldsymbol{U}}_{nm}^B + k_{\text{eff}}(1+\alpha)\boldsymbol{V}_m\boldsymbol{C}\tilde{\boldsymbol{U}}_n^B = -k_{\text{eff}}\tilde{\Delta}_n\boldsymbol{V}_m \tag{S21}$$

There are six equilibrium equations for each *m*. Considering *m*=0, 1⋯, *M*, the equations become,

$$\left(\boldsymbol{K}_n + k_{\text{eff}}(1+\alpha)\boldsymbol{V}\boldsymbol{C}\right)\tilde{\boldsymbol{U}}_n^B = -k_{\text{eff}}\tilde{\Delta}_n\boldsymbol{V} \tag{S22}$$

where,

$$\boldsymbol{K}_n = \mathrm{diag}\left(\boldsymbol{K}_{n0}, \boldsymbol{K}_{n1}, \cdots, \boldsymbol{K}_{nM}\right) \tag{S23}$$

$$\boldsymbol{V} = \left\{\boldsymbol{V}_0, \boldsymbol{V}_1, \cdots, \boldsymbol{V}_M\right\}^{\mathrm{T}} \tag{S24}$$

There are 6(M+1) equilibrium equations in Eq. (S22) to uniquely determine the known vector $\tilde{\boldsymbol{U}}_n^B$. Considering each wavenumber n and response frequency ω, the displacements of the tunnel and soil in the time-space domain are calculated using Eqs. (11) and (12). The value of M will affect both the accuracy and efficiency of the predictions. When M is set to 8, the prediction results reach convergence.

S1.4 Analytical solution of floating slab

As stated above, the floating slab is treated as a continuous slab in this study and is modeled as an infinitely long Euler beam as well, as shown in Fig. S4. It is worth noting that the rubber pad beneath the floating slab is represented as a continuous spring. Additionally, the discrete supports of the floating slab can be simplified as a continuous spring.

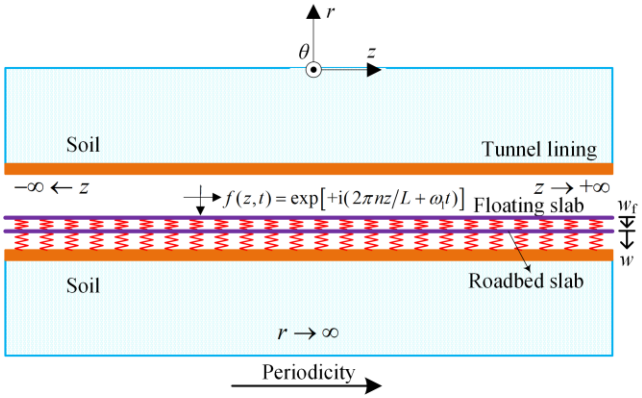

Fig. S4 Floating slab track attached to the tunnel invert in the periodic PiP model.

Similarly, the equilibrium equations for the roadbed and floating slab beams have the following form,

$$m\frac{\partial^2 w}{\partial t^2} + EI\frac{\partial^4 w}{\partial z^4} + k_{\mathrm{eff}}\left(w + W^{\dagger}\right) + k_{\mathrm{f}}\left(w - w_{\mathrm{f}}\right) = 0 \tag{S25}$$

$$m_{\mathrm{f}}\frac{\partial^2 w_{\mathrm{f}}}{\partial t^2} + EI_{\mathrm{f}}\frac{\partial^4 w_{\mathrm{f}}}{\partial z^4} + k_{\mathrm{f}}\left(w_{\mathrm{f}} - w\right) = f(z,t) \tag{S26}$$

where the subscript f represents the quantity for the floating slab.

By applying a Fourier transform regarding t and a modal decomposition regarding z to Eq. (S25), the solution has the following form,

$$\tilde{w}_n = \alpha_1 \tilde{w}_{\mathrm{f}n} + \tilde{\Delta}_{1n}\tilde{W}_n^{\dagger} \tag{S27}$$

$$\alpha_1 = \frac{k_{\mathrm{f}}}{EI\lambda_n^4 - m\omega^2 + k_{\mathrm{eff}} + k_{\mathrm{f}}}, \tilde{\Delta}_{1n} = \frac{-k_{\mathrm{eff}}}{EI\lambda_n^4 - m\omega^2 + k_{\mathrm{eff}} + k_{\mathrm{f}}} \tag{S28}$$

Similar manipulations to Eq. (S26), another solution can be obtained,

$$\tilde{w}_{\mathrm{f}n} = \alpha_2 \tilde{w}_n + \tilde{\Delta}_{2n} \tag{S29}$$

$$\alpha_2 = \frac{k_\mathrm{f}}{EI_\mathrm{f}\lambda_n^4 - m_\mathrm{f}\omega^2 + k_\mathrm{f}}, \tilde{\Delta}_{2n} = \frac{\tilde{f}_n}{EI_\mathrm{f}\lambda_n^4 - m_\mathrm{f}\omega^2 + k_\mathrm{f}} \tag{S30}$$

Substituting Eq. (S29) into Eq. (S27), the following equation is derived by eliminating the quantity $\tilde{w}_{\mathrm{f}n}$,

$$\tilde{w}_n = \tilde{W}_n^{\dagger}\alpha^* + \tilde{\Delta}_n^* \tag{S31}$$

$$\alpha^* = \frac{\tilde{\Delta}_{1n}}{1-\alpha_1\alpha_2}, \tilde{\Delta}_n^* = \frac{\alpha_1\tilde{\Delta}_{2n}}{1-\alpha_1\alpha_2} \tag{S32}$$

By comparing Eq. (S32) with Eq. (S14), it is evident that the formulations of both equations are identical. This indicates that the coupling between the floating slab track with the tunnel invert is the same as that between the regular slab track with the tunnel invert, as formulated by Eqs. (S16)-(S24). Accordingly, the derivations will not be repeated here.

S1.5 Train load expression in the frequency-wavenumber domain

As stated, the supporting forces, specifically the train loads in this study, are applied discretely to both the regular track slab and the floating slab, each featuring a periodicity length of L=0.6 m, as illustrated in Fig. S5. The supporting forces are determined using the analytical model for periodic train-track and train-floating slab track interactions developed by Ma (2015). In the floating slab track model (Ma, 2015), the floating slab is treated as an infinitely long beam, and the discrete supports beneath the slab are approximated as a continuous spring.

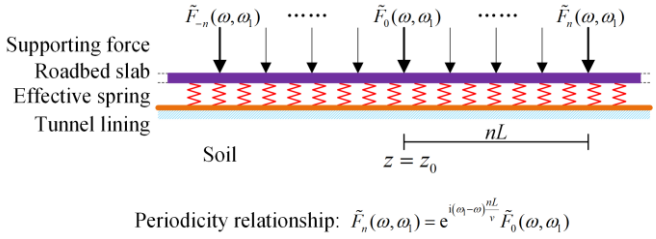

(a) Train load on the regular track slab

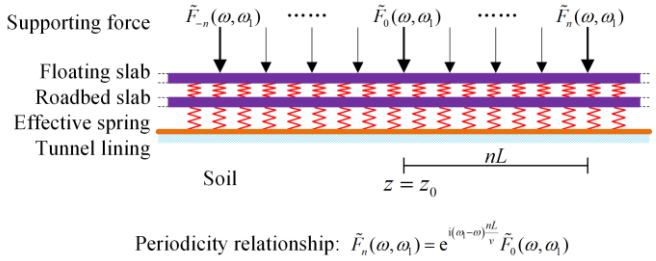

(b) Train load on the floating slab

Fig. S5 Supporting forces periodically exerted on the (a) regular track slab and (b) floating slab.

Ma (2015) has demonstrated that supporting forces $\tilde{F}_0(\omega,\omega_1)$ and $\tilde{F}_n(\omega,\omega_1)$ at z=z_0 and z=z_0+nL follow this periodicity relationship,

$$\tilde{F}_n(\omega,\omega_1) = \mathrm{e}^{\mathrm{i}(\omega_1-\omega)\frac{nL}{v}}\tilde{F}_0(\omega,\omega_1) \tag{S33}$$

Thus, the total forces acting on the slab are the sum of supporting forces $\tilde{F}_n(\omega,\omega_1)$,

$$\tilde{f}\left(z,\omega,\omega_1\right)=\sum_{n=-\infty}^{n=+\infty}\delta\left(z-z_0-nL\right)\mathrm{e}^{\mathrm{i}(\omega_1-\omega)\frac{nL}{v}}\tilde{F}_0\left(\omega,\omega_1\right) \tag{S34}$$

The function $\tilde{f}\left(z,\omega,\omega_1\right)$ adheres to the following relationship,

$$\tilde{f}\left(z+nL,\omega,\omega_1\right)=\mathrm{e}^{\mathrm{i}(\omega_1-\omega)\frac{nL}{v}}\tilde{f}\left(z,\omega,\omega_1\right) \tag{S35}$$

By applying the periodicity feature and the discrete Fourier transform, the expressions for $\tilde{f}\left(z,\omega,\omega_1\right)$ and its modal components $\tilde{f}_n\left(\omega,\omega_1\right)$ are,

$$\tilde{f}\left(z,\omega,\omega_1\right)=\frac{\tilde{F}_0\left(\omega,\omega_1\right)}{L}\sum_{n=-\infty}^{n=+\infty}\mathrm{e}^{\mathrm{i}\left(\frac{2\pi n}{L}+\frac{\omega_1-\omega}{v}\right)(z-z_0)} \tag{S36}$$

$$\tilde{f}_n\left(\omega,\omega_1\right)=\frac{\tilde{F}_0\left(\omega,\omega_1\right)}{L}\mathrm{e}^{-\mathrm{i}\left(\frac{2\pi n}{L}+\frac{\omega_1-\omega}{v}\right)z_0} \tag{S37}$$

Substituting Eq. (S37) into Eqs. (S15) and (S30), the dynamic response of the tunnel lining and soil can be predicted quickly by Eq. (S22). It should be noted that the calculation should be repeated with respect to n, ω, and ω_1. To further enhance the prediction efficiency, two measures of the calculation efficiency improvement can be applied to reduce the calculation loops (Ma et al., 2024).

Section S2. Model validation and verification

S2.1 Additional Model parameter

The fastener supporting forces from metro trains are calculated using the analytical models (Ma, 2015). The metro train consists of six carriages, with each carriage containing one car, two bogies, and four wheelsets. Table S1 gives the calculation parameters for the metro train. Type-60 rails are modeled as infinitely long Euler beams, which are periodically supported (L=0.6 m) by the $DTVI_2$ fastener system. Table S2 presents the mechanical parameters for the rails and fasteners, corresponding to the results of two parallel rails.

Table S1 Main parameters for metro train.

Carriage parameters	Values
Individual carriage length	19 m
Individual car body mass	4.3×10^4 kg
Car body mass inertia moment	1.7×10^6 kg·m^2
Individual bogie mass	3.6×10^3 kg
Bogie mass inertia moment	9.62×10^3 kg·m^2
Spacing between bogies	12.6 m
Individual wheelset mass	1.7×10^3 kg
Spacing between wheelsets	2.2 m
Primary suspension stiffness	1.4×10^6 N/m
Primary suspension damping	5×10^4 N·s/m

Secondary suspension stiffness	5.8×10^5 N/m
Secondary suspension damping	1.6×10^5 N·s/m

Table S2 Mechanical parameter for rail and fastener.

Parameters	Values
Fastener vertical stiffness	1.2×10^8 N/m
Fastener vertical damping	6×10^4 N·s/m
Spacing between adjacent fastener	0.6 m
Rail mass per unit length	121.28 kg/m
Rail elastic modulus	2.059×10^{11} N/m^2
Rail inertia moment of cross section	6.434×10^{-5} m^4
Rail loss factor	0.01

S2.2 Measured vibration source intensities

The measured vibration source intensities are listed in Table S3. It can be found that the measured results predominantly fall within the range of 77.1 to 87.5 dB, exhibiting a noticeable level of uncertainty. These results will be used to validate the proposed model.

Table S3 Measured vibration source intensity in Beijing

Section	Speed (km/h)	Intensity (dB)	Section	Speed (km/h)	Intensity (dB)
1	80	77.1	7	72	79.7
2	57	82.4	8	68	84.5
3	69	85.9	9	68	87.5
4	76	82	10	60.4	82.5
5	78	81.6	11	70	80
6	69	78.8			

S2.3 Additional description of Fig. 9 in the manuscript

It can be found from the results of the present model in Fig. S6a that the time history reveals the passing process of the metro train, with multiple peaks being excited by the impact of the train wheel, reaching a maximum acceleration of 0.1486 m/s^2. From Fig. 6b, due to the resonance of the unsprung mass on the track and the short-wavelength track irregularities, vertical vibrations at the tunnel wall mainly spread within 50-70 Hz. Another peak is observed within 20-40 Hz, corresponding to the frequency $f=v/L$=27.8 Hz. Vertical vibrations in the one-third octave band exhibit a dominant frequency of 63 Hz, attributed to the dynamic coupling between the train and the track. In Fig. S6d, the vertical vibration level versus time is depicted, showing the peak vibration level occurring within 2-8s with a value of 81.5 dB. By employing the proposed model, it is possible to gather comprehensive information regarding the vibration source in both the time and frequency domains.

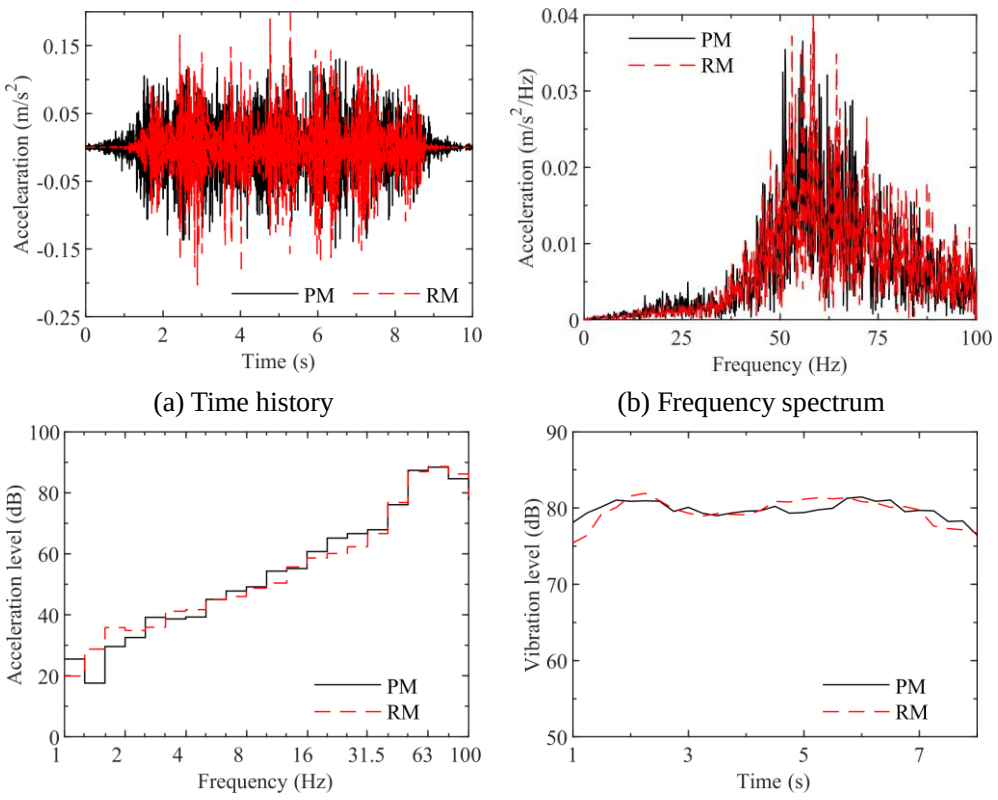

(a) Time history (b) Frequency spectrum

(c) One-third octave (d) Vibration level

Fig. S6 Typical vibration results at the tunnel wall for v=60 km/h, S1, and Q2: (a) time history, (b) frequency spectrum, (c) one-third octave band, and (d) vibration level.

Section S3 Additional result and discussion

S3.1 Isolation effect of floating slab track

In Fig. S7, comparisons are made between the typical results of the vibration source using regular and floating slab tracks under the train speed v=60 km/h, soil S1, and track irregularities Q2. The noticeable vibration mitigation effects can be observed with the use of a floating slab track. In the time history, the peak acceleration response decreases significantly from 0.1486 m/s^2 to 0.0091 m/s^2, representing a reduction of approximately 93.9%. In the frequency spectrum, the vibration amplitude experiences a significant decrease across most frequencies, particularly at the dominant frequency. Nevertheless, there is an amplification of vibration around 8 Hz, which corresponds to the first-order natural frequency $f_{\mathrm{f}} = \dfrac{1}{2\pi}\sqrt{\dfrac{k_{\mathrm{f}}}{m_{\mathrm{f}}}} = 8.6$ Hz. These phenomena are clearly evident in the one-third octave band analysis, showing a maximum reduction of the acceleration level by 29.7 dB at 63 Hz and an increase of 12.9 dB at 8 Hz. From Fig. S7d, it is evident that the floating slab track exhibits a significant vibration isolation capability, with the maximum reduction in vibration source intensity being 12.8 dB.

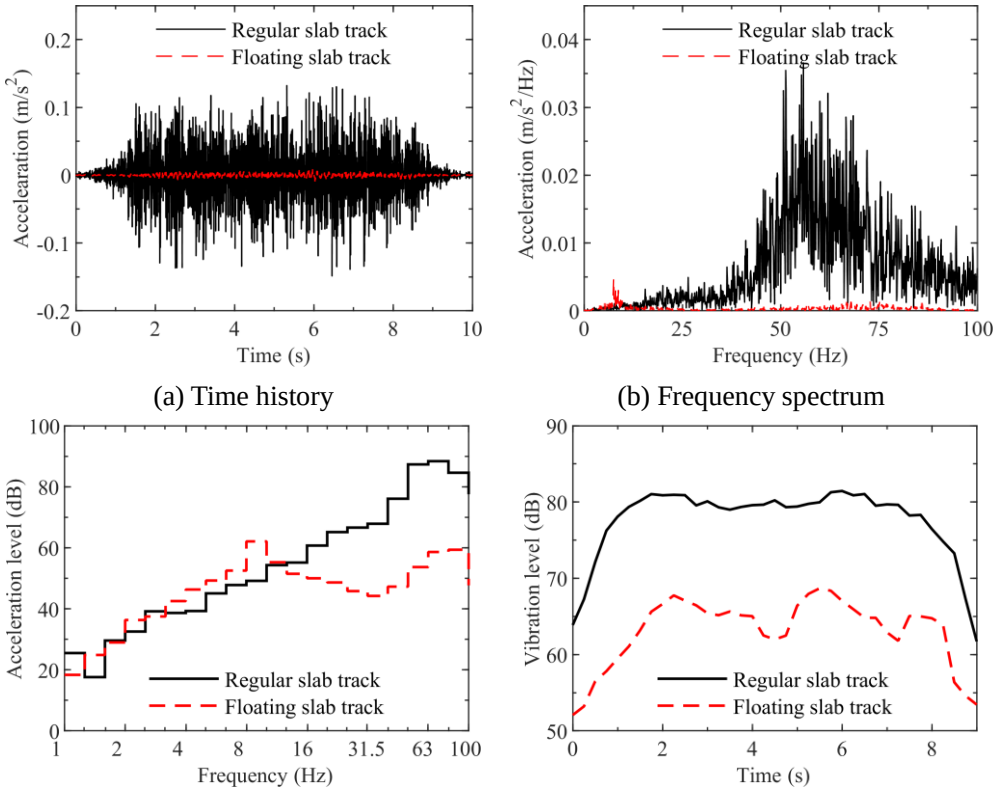

(a) Time history (b) Frequency spectrum

(c) One-third octave (d) Vibration level

Fig. S7 Typical result of vibration source with regular and floating slab track for v=60 km/h, S1, and Q2: (a) time history, (b) frequency spectrum, (c) one-third octave band, and (d) vibration level.

S3.2 Discussion

The primary contribution of this work is the extension of the traditional PiP model to address the periodicity arising from the periodic arrangement of discretely distributed fasteners. This approach allows for the straightforward inclusion of the slab beam in the analytical model. Additionally, the support forces derived from the periodic train-track and train-floating slab track interactions, as developed by Ma (Ma, 2015), are analytically decomposed in the frequency-wavenumber domain and incorporated into the proposed model.

The proposed method predicts the vibration source intensity in just 58 s using the 13th Gen Intel(R) Core(TM) i7-13700K 3.40 GHz CPU processor, which is remarkably quick compared to the previously established tunnel-soil coupled analytical model (Ma et al., 2024), which takes 3 h. It should be highlighted that the advantage of the periodic tunnel-soil coupled analytical model lies in quick ground vibration prediction, while the model presented in this paper excels in rapidly predicting vibration source intensity induced by metro trains.

The validation and verification confirm its accuracy. This indicates that when comparable measurements or database predictions of vibration source intensity are unavailable, this method can serve as a complementary approach to determine the vibration source intensity accurately and efficiently for empirical assessments of environmental vibration. Additionally, this method can be employed to evaluate the vibration mitigation effectiveness of the floating slab track.

References

Flügge W, 1973. Stresses in Shells (the 2nd edition). Berlin, Springer.

Forrest JA, Hunt HEM, 2006. A three-dimensional tunnel model for calculation of train-induced ground vibration. *J Sound Vib*, 294(4-5): 678-705. https://doi.org/10.1016/j.jsv.2005.12.032

Hussein MFM, François S, Schevenels M, et al., 2014. The fictitious force method for efficient calculation of vibration from a tunnel embedded in a multi-layered half-space. *J Sound Vib*, 333(25): 6996-7018. https://doi.org/10.1016/j.jsv.2014.07.020

Ma LX, 2015. Study on the model of coupled vehicle & track and the analysis model for tunnel-ground vibration response based on the periodic-infinite structure theory [PhD thesis in Chinese]. Beijing Jiaotong University, Beijing.

Ma M, Xu L, Liu W, et al., 2024. Semi-analytical solution of a coupled tunnel-soil periodic model with a track slab under a moving train load. *Appl Math Model*, 128: 588-608. https://doi.org/10.1016/j.apm.2024.01.038

Xu L, Ma M, 2023. Analytical solution of ground-borne vibration due to a spatially periodic harmonic moving load in a tunnel embedded in layered soil. *J Zhejiang Univ-Sci A*, 24(7): 637-652. https://doi.org/10.1631/jzus.A2200385